What are the Driving Factors Influencing the Size Distribution of Airborne Synthetic Clay Particles Emitted from a Jet Milling Process?

Ehsan Majd Faghihi[1], Darren Martin[2], Farhad Salimi[3], Grant Edwards[2], Congrong He[1], Lidia Morawska[1*]

[1] International Laboratory for Air Quality and Health, Queensland University of Technology, GPO Box 2434, Brisbane QLD, 4001, Australia
[2] Australian Institute for Bioengineering and Nanotechnology (AIBN), The University of Queensland, Brisbane QLD, 4072, Australia
[3] Menzies Research Institute, University of Tasmania, Hobart TAS, 7000, Australia

ABSTRACT

In the field of workplace air quality, measuring and analyzing the size distribution of airborne particles to identify their sources and apportion their contribution has become widely accepted, however, the driving factors that influence this parameter, particularly for nanoparticles (< 100 nm), have not been thoroughly determined. Identification of driving factors, and in turn, general trends in size distribution of emitted particles would facilitate the prediction of nanoparticles' emission behavior and significantly contribute to their exposure assessment. In this study, a comprehensive analysis of the particle number size distribution data, with a particular focus on the ultrafine size range of synthetic clay particles emitted from a jet milling machine was conducted using the multi-lognormal fitting method. The results showed relatively high contribution of nanoparticles to the emissions in many of the tested cases, and also, that both surface treatment and feed rate of the machine are significant factors influencing the size distribution of the emitted particles of this size. In particular, applying surface treatments and increasing the machine feed rate have the similar effect of reducing the size of the particles, however, no general trend was found in variations of size distribution across different surface treatments and feed rates. The findings of our study demonstrate that for this process and other activities, where no general trend is found in the size distribution of the emitted airborne particles due to dissimilar effects of the driving factors, each case must be treated separately in terms of workplace exposure assessment and regulations.

Keywords: Airborne particle emission; Size distribution; Workplace aerosol measurement.

INTRODUCTION

There is now a growing consensus over the impact of airborne engineered particles' size on their toxicity and behavior in different environments (Maynard and Kuempel, 2005; Donaldson *et al.*, 2006; Asbach *et al.*, 2009). Thus, determining the size distribution of these particles during different stages of their life cycle, particularly in nanotechnology workplaces where the amount of the emitted particles is significant and many people are exposed to them, is of crucial importance. This task requires isolating the particles of interest from any other interfering factors (i.e., background particles and those emitted from other activities in the area where measurement takes place), discriminating them based on their size, and finally quantifying the particles in each size bin (Ramachandran and Cooper, 2011). Researchers have employed instruments operating on several different principles and/or size ranges for aerosol size distribution measurements (Maynard and Aitken, 2007; Ono-Ogasawara *et al.*, 2009). A review of the literature suggests that in order to measure the particle size distribution within a wide range from a few nanometers to several micrometers, a combination of the Scanning Mobility Particle Sizer (SMPS) (Demou *et al.*, 2008; Tsai *et al.*, 2011) or the Fast Mobility Particle Sizer (FMPS) (Tsai *et al.*, 2008, 2009) with the Optical Particle Counter (OPC) (Methner *et al.*, 2010; Park *et al.*, 2011) or the Aerodynamic Particle Sizer (APS) (Koponen *et al.*, 2010; Schlagenhauf *et al.*, 2012) is required. The list of the conducted studies in various nanotechnology workplaces, alongside the methods/instruments that were used to measure the size distribution of the emitted particles due to different activities can be found in several review papers including those published by (Brouwer *et al.*, 2009; Brouwer, 2010) and

---
* Corresponding author.
 Tel.: +61-7-3138 2616; Fax: +61-7-3138 9079
 E-mail address: l.morawska@qut.edu.au

(Kuhlbusch *et al.*, 2011).

Despite the fact that size distribution was often included in workplace aerosol measurements, the majority of studies were concerned with the effect of adding different nanofillers to the reference materials on the properties of the emitted particles (including their size distribution (Bello *et al.*, 2009; Göhler *et al.*, 2010; Koponen *et al.*, 2010; Sachse *et al.*, 2012)). So far, however, very few studies have attempted to quantitatively characterize particle size distribution and to study the effects of different factors on this key parameter.

According to the literature, aerosol particle size distribution can be represented by a sum of several log-normal distributions (Hussein *et al.*, 2005). Although the method was initially used for atmospheric aerosols, some researchers have applied it to engineered nanoparticles as well. For instance, Schlagenhauf *et al.* (2012) studied the abrasion process of epoxy-based nanocomposites containing carbon nanotubes using this method and showed that all tested samples had four modes, among which the smallest size was measured by SMPS, and the remaining three by APS. In another study, Koponen *et al.* (2009, 2010) reported that the dust emission from sanding nanoparticle-containing paints consisted of five size modes, with the first three under 1 μm and the other two around 1 and 2 μm.

One particular class of materials that has gained an increasing popularity in industrial use due to its superior physical properties compared to the natural clays is the synthetic clays (Stoeffler *et al.*, 2008). Nevertheless, only a handful of studies have been conducted on the emission of nanoparticles from these materials during different activities, or on the physio-chemical characterization of such particles (Suh *et al.*, 2009; Sachse *et al.*, 2012).

The overall aim of this study was to infer the emission characteristics of a range of jet milled synthetic clay particles by studying their size distributions under various conditions, i.e., following the application of different surface treatments to the feed materials or varying of the feed rate, with a particular interest in nanoparticles. Our approach was to assess factors driving the emission of the airborne submicrometer particles from the abovementioned process, followed by investigating the effect of these parameters on the size distribution of the emitted particles using the multi-lognormal fitting method. The main objectives of

this study were to:

● Determine the contribution of different size ranges to the total size distribution of the emitted airborne particles from this mechanical process
● Establish the extent to which the size distribution of the emitted particles, in both sub and super-micrometer range, is influenced by surface treatment and feed rate of the milling machine
● Assess whether the effect of surface treatment on size distribution is similar across different materials

METHODS

Process

Measurements were conducted in a university laboratory, using a Micron-Master Jet Pulverizer jet milling machine to reduce the size of the synthetic clay composites by grinding the feed material. The working principle of the process is based upon the particle collision. Whilst the large particles are held in the grinding chamber by the centrifugal force, the ground particles are carried out by an air flow and collected in the product chamber. More information can be found in our previous study (Faghihi *et al.*, 2015).

Materials Tested

Four types of synthetic clays with different primary particle/agglomerate sizes were used. In addition to these unmodified samples, each one was subjected to five different surface treatments, which were obtained by applying different ratios of the two main surface treatments Choline Chloride (CC) and Ethoquad O/12 PG (ETHO), bringing the total number of the study cases to 24. Table 1 summarizes the properties of these synthetic clays.

Instrumentation

To capture a wide range of particle size, the TSI AERO TRAK model 9306 Optical Particle Counter (OPC) with size range of 0.3–10 μm and flow rate of 2.8 L min^{-1} was used. The OPC bin sizes used in this study were 0.3–0.5, 0.5–1, 1–3, 3–5, 5–10, and >10 μm. For the submicrometer size range, the ideal measurement instrument capable of capturing all the momentary variations in size distribution is FMPS. However, since we did not have access to this instrument at the time of conducting this study, a SMPS

Table 1. Properties of the synthetic clay types and the applied surface treatments.

Material	Primary particle/agglomerate size (nm)	Main surface treatment	Molecular mass (g mol^{-1})	Applied surface treatment	CC/ETHO mixing ratio (%)
Lucentite® (LUC)	25	Choline Chloride (CC)	139.6	N (non)	-
Laponite® (H80)	80			CC	100/0
				CMOD	75/25
Laponite® (H120)	120	Ethoquad O/12 PG (ETHO)	406.1	MMOD	50/50
				EMOD	25/75
Cloisite® (CLO)	300			ETHO	0/100

consisting of a TSI long DMA (Differential Mobility Analyzer) model 3081 and a TSI CPC (Condensation Particle Counter) model 3782, which measured in the size range of 10–422 nm was used. Previous studies conducted on other mechanical processes such as abrasion (Schlagenhauf *et al.*, 2012) and sanding (Göhler *et al.*, 2010) did not report any significant emission of nanoparticles smaller than 10 nm. Therefore, and due to the similar mechanical nature of the jet milling process in the present study, the abovementioned size range was deemed to be appropriate for characterization of nanoparticle emission from this process. The up-scan time was set to 120 s followed by a down-scan of 30 s. The sheath and aerosol air flow of the classifier were set to 6 and 0.6 L min^{-1}.

At the beginning of each measurement day, the flow rates of the instruments were checked by a bubble flow meter and their times were synchronized. The sampling frequency of the OPC was set to the shortest time possible (1 s) to measure all the momentary variations during size distribution measurements. The SMPS was calibrated prior to conducting the measurements using monodisperse polystyrene latex (PSL) particles with the nominal diameter of 46 nm. A zero check of all instruments was also performed at the beginning of each day of measurements using a high-efficiency particulate air (HEPA) filter.

Study Design

Firstly, by comparing the instruments' readings in the vicinity of the jet milling machine before and during its operating time, it was confirmed that the source of airborne particle emission was at the connection point of the collection bag to the venturi outlet. A black conductive rubber tube was placed in the proximity of the particle emission source (ca. 2 cm) with its other end connected to an aerosol flow splitter, which was used to feed both the OPC and SMPS. To minimize particle losses, the shortest possible lengths were used for tubing (< 20 cm). Furthermore, the effect of particle loss inside the connecting tube due to the diffusion was calculated based on the method presented by (Hinds, 2012). The results showed than only less than 4% of particles smaller than 20 nm in diameter were lost in the tube, confirming that particle loss could be assumed negligible in this case.

For each of the available 24 samples, SMPS scans (150 s each) were conducted in triplicate. Despite minor discrepancies across them, the scans were fairly similar in terms of the key characteristics of the modes, confirming the reliability of the obtained results. After this period, the machine was turned off, dismantled and cleaned for the next sample. Whilst studying the effect of the surface treatments, the feed rate of the jet milling machine was kept constant.

To assess the effect of the feed rate on the size distribution of the emitted particles, three feed rates (7.5, 4.1 and 2.1 g min^{-1}) were applied to two different samples (LUC-N and H80-EMOD).

Data Analysis

Both OPC and SMPS data were imported into R programming and statistical computing software (R.Core.Team, 2013). The background PNSDs (Particle Number Size Distributions) at the emission source, during the operation of the jet milling machine and before adding the product to it, were measured by SMPS and OPC, averaged, and then subtracted from the measured PNSDs during the milling process to represent the product emission. Combining SMPS and OPC data, in view of the differences in their measurement techniques, has been done in some other studies such as the one published by (Park *et al.*, 2011), where the data from these instruments were combined to calculate reference surface area concentration.

The OPC data were used to obtain an overview of the size distribution in a wide range by examining the number concentration in each size bin, as well as the number concentration of super-micrometer particles. As mentioned earlier, the major focus of this study was on the nanoparticles. Therefore, the main effort in analyzing the data was dedicated to them. Initially, three scans for each sample were replaced by their mean, leading to a data set of 24 size distributions. The data were then smoothed by fitting a Generalized Additive Model (GAM) in R, based on penalized B-splines (Eilers and Marx, 1996; Wood, 2003) to eliminate the noises in the PNSD spectra. Using the Multi-peak Fitting package in Igor Pro 6.21 (WaveMetrics), the data for each sample were replaced by the following multi-lognormal fit:

$$Y = Y_0 + A \exp\left[-\left(\frac{\ln\left(\frac{x}{x_0}\right)}{W} \right)^2 \right] \tag{1}$$

The fit returned Y_0, A, x_0, and W for each mode in PNSD. By comparing Eq. (1) with the mathematical expression of the multi-lognormal distribution, the key properties of each mode were obtained as below:

$$\begin{cases} D_P = x_0 \\ \sigma = \exp\left(\frac{W}{\sqrt{2}}\right) \\ N = \sqrt{2\pi}.A.\log\sigma \end{cases} \tag{2}$$

These parameters are geometric mean diameter D_P, geometric standard deviation σ, and mode number concentration N and were used to determine the number and location of the modes in each size range and to identify their contribution to the emission of each sample from the process. These values were then compared across the samples in an attempt to understand the effect of surface treatment and machine feed rate in the emission of synthetic clay particles from the studied milling process.

RESULTS AND DISCUSSION

Total Particle Number Concentration (PNC)

Table 2 presents the individual background and process

Table 2. Mean background and process concentrations for individual samples and their standard deviations in parenthesis, together with total number concentrations of emitted clay particles and background.

| Material | Surface treatment | SMPS (cm^{-3}) | | OPC (cm^{-3}) | | Product emission (cm^{-3}) ($\times 10^3$) | Background concentration (cm^{-3}) ($\times 10^2$) |
		Background ($\times 10^2$)	Process ($\times 10^3$)	Background	Process ($\times 10^2$)		
LUC	N	9.2 (0.4)	1.3 (0.4)	1 (1)	2.6 (0.3)	0.6	9.2
	CC	10.5 (1.6)	2.1 (0.5)	6 (1)	2.4 (0.7)	1.3	10.5
	CMOD	8.8 (1.5)	1.1 (0.3)	1 (0)	0.6 (0.1)	0.3	8.8
	MMOD	6.3 (0.8)	2.4 (0.4)	9 (2)	2.0 (0.3)	2.0	6.4
	EMOD	4.6 (0.9)	1.6 (0.8)	3 (1)	1.1 (0.4)	1.3	4.6
	ETHO	3.7 (0.4)	1.6 (0.8)	2 (1)	0.8 (0.2)	1.3	3.7
H80	N	4.9 (0.1)	3.1 (1.1)	1 (0)	2.5 (0.3)	2.9	4.9
	CC	3.7 (0.6)	1.2 (0.2)	4 (0)	0.5 (0.1)	0.9	3.7
	CMOD	3.9 (0.4)	12.6 (1.9)	5 (1)	2.6 (0.7)	12.5	3.9
	MMOD	2.7 (0.3)	6.8 (1.0)	5 (1)	3.7 (0.5)	6.9	2.8
	EMOD	5.5 (0.3)	2.6 (0.6)	2 (0)	2.9 (0.4)	2.3	5.5
	ETHO	4.5 (0.6)	6.8 (1.1)	1 (0)	7.0 (0.6)	7.1	4.5
H120	N	3.0 (0.5)	20.1 (1.9)	1 (0)	7.6 (0.3)	21.0	3.0
	CC	2.9 (0.3)	8.4 (0.9)	3 (1)	3.8 (0.6)	8.5	2.9
	CMOD	1.8 (0.3)	1.8 (0.1)	1 (1)	1.1 (0.1)	1.7	1.8
	MMOD	2.9 (0.3)	2.6 (0.8)	3 (1)	1.6 (0.2)	2.4	3.0
	EMOD	1.8 (0.2)	3.9 (0.5)	1 (0)	1.5 (0.3)	3.8	1.8
	ETHO	2.1 (0.1)	5.0 (1.1)	1 (0)	1.7 (0.7)	5.0	2.1
CLO	N	2.4 (0.3)	26.0 (1.7)	5 (0)	4.5 (1.2)	26.2	2.5
	CC	3.8 (0.1)	6.1 (0.9)	1 (0)	2.6 (0.6)	5.9	3.8
	CMOD	3.8 (0.3)	7.8 (0.4)	2 (1)	4.4 (0.9)	7.9	3.8
	MMOD	2.6 (0.3)	3.8 (0.5)	3 (2)	2.5 (0.2)	3.8	2.6
	EMOD	1.8 (0.2)	3.7 (0.9)	1 (0)	1.7 (0.3)	3.7	1.8
	ETHO	4.2 (0.2)	2.0 (0.4)	7 (1)	2.1 (0.1)	1.8	4.3

total PNCs measured by SMPS and OPC, as well as the total concentrations for product and background for each sample. "Background" and "Process" refer to the stages, when the milling machine was running without and with the feed material, respectively. Therefore, the difference of the mean PNCs between process and background yields the concentration of the emitted clay particles, i.e., product emission.

Comparison of the individual SMPS and OPC total number concentrations in Table 2 shows that the emitted clay particles were dominated by those in the sub-micrometer range, particularly d < 0.3 μm, which is the SMPS data range used in this study. The mean total PNC of the background was 4.3×10^2 cm^{-3} with a SD of 2.4×10^2 cm^{-3}. Similar to the emitted clay particles, background particles were also mainly in the range of d < 0.3 μm. Total PNC of the emitted clay particles were obtained by subtracting the background concentration from the process concentration for both SMPS and OPC and summing the results. It varied in the range of $0.3–26.2 \times 10^3$ cm^{-3}.

Among the particle sizes, concentrations of LUC samples obtained by both SMPS and OPC, and consequently, the total concentration were the lowest. On the other end of the spectrum, CLO samples had the highest overall SMPS number concentration and the second highest overall OPC number concentration after H80. Therefore, this particle size exhibited the highest average total concentration. The

variations of concentration across different surface treatments within each size were not identical. For instance, whilst for H120 and CLO, the emission of the unmodified samples was significantly higher than others, for H80, MMOD treatment showed the highest emission.

This initial assessment highlighted a need to investigate the PNSD of the emitted clay particles more closely, mainly in the SMPS size range, which includes ultrafine particles.

Particle Number Size Distributions (PNSDs)
Smoothing the PNSD Spectra

Fig. 1 shows the smoothed mean PNSDs of background, process including background, and emitted clay particles for sample H120-ETHO, as an example for the application of GAM fit in this study. As can be seen, background particle concentration is very low. It remained almost unchanged for other tested samples due to the effective ventilation of the experiment location, which provided a fairly clean environment.

Together with the total number concentration results in Table 2, Fig. 1 provides solid evidence for the emission of clay particles from this process by showing a significant difference between background and product concentrations. As can be seen in Fig. 1, the PNSD for the emitted clay particles includes multiple modes corresponding to both nanoparticles and particles of bigger sizes (> 100 nm). Another noteworthy point regarding Fig. 1 is that correcting
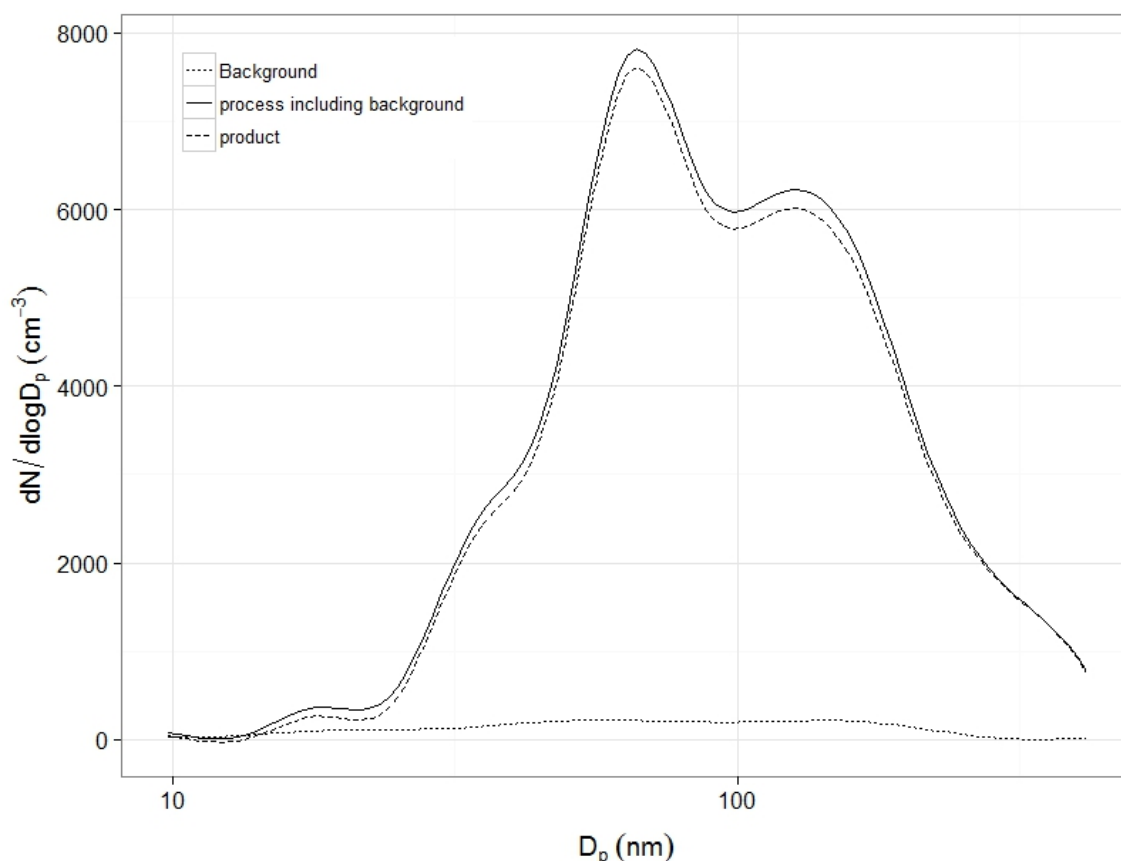
Fig. 1. Smoothed PNSDs of H120-ETHO during different measurement stages, obtained by applying GAM fit.

the measured PNSD for that of background did not affect the properties of these modes, and their shapes and locations were preserved.

Multi-Lognormal Fitting

In order to quantify the effect of surface treatment and feed rate on the size distribution of the emitted particles, a multi-lognormal fit was applied to the PNSD spectrum of each sample. This section starts with studying the effect of surface treatment and will proceed to evaluation of milling feed rate as another parameter of potential impact.

The difference between concentrations of measured and fitted data did not exceed 10%, hence, confirming the suitability of the applied multi-lognormal fits. Fig. 2 shows the results of applying the fit to the PNSD spectra of CLO samples.

It can be inferred from Fig. 2 that the multi-lognormal fits are suitable for parameterization of PNSDs, as they can be fitted to the obtained experimental data within an acceptable level of accuracy. The resultant parameters can then be used to facilitate the characterization of the emitted particles in the size range corresponding to SMPS. This method was applied to all PNSDs and the important characteristics of the modes were obtained. GMD (Geometric Mean Diameter) and total number concentration of the modes are presented in Fig. 3.

From Fig. 3, it can be seen that despite different primary sizes, all tested cases had not only one, but in most cases

two nanoparticle modes. Among the tested materials, LUC and CLO samples had 11 nanoparticle modes, whilst H80 and H120 had 10. In order to thoroughly determine the effect of surface treatment on size distribution of the emitted nanoparticles, the following assessment criteria were chosen: location of nanoparticle modes, variations in the location of nanoparticle mode(s) for each material due to different surface treatments, and the contribution of nanoparticles to the total emissions.

Location of nanoparticle modes: According to Fig. 3, the overall impact of applying surface treatments to the available materials on the size distribution of the emitted particles was emission of smaller particles. Except for a few cases, the results show a shift toward smaller sizes in both nanoparticle and larger modes of the emitted particles in the surface-treated materials compared to the unmodified ones. A closer look into Fig. 3 shows an overall declining trend in the geometric mean diameters of the first two modes across surface treatments from N to ETHO. A possible explanation for this phenomenon could be collision of the particles. As stated earlier, the particles collide with one another at very high velocities and get pulverized inside the grinding chamber of the jet milling machine. Because the surface-treated particles are heavier and have more kinetic energy compared to the unmodified ones, their collision could result in a more significant size reduction of the particles. Despite this overall declining trend in size with surface treatment, this parameter also shows some dissimilar effects
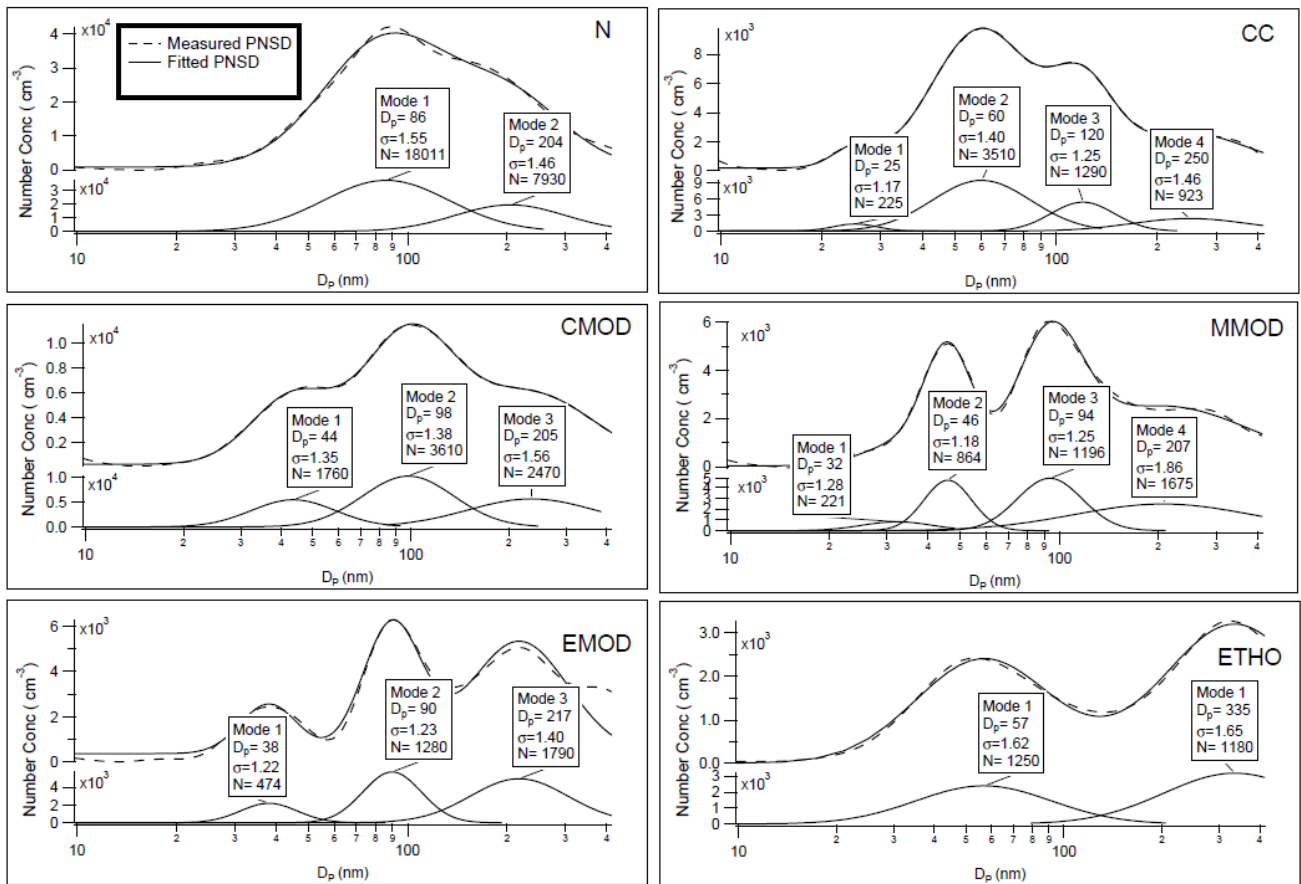
Fig. 2. Results of the multi-lognormal fits applied to the PNSD of CLO samples measured by SMPS.
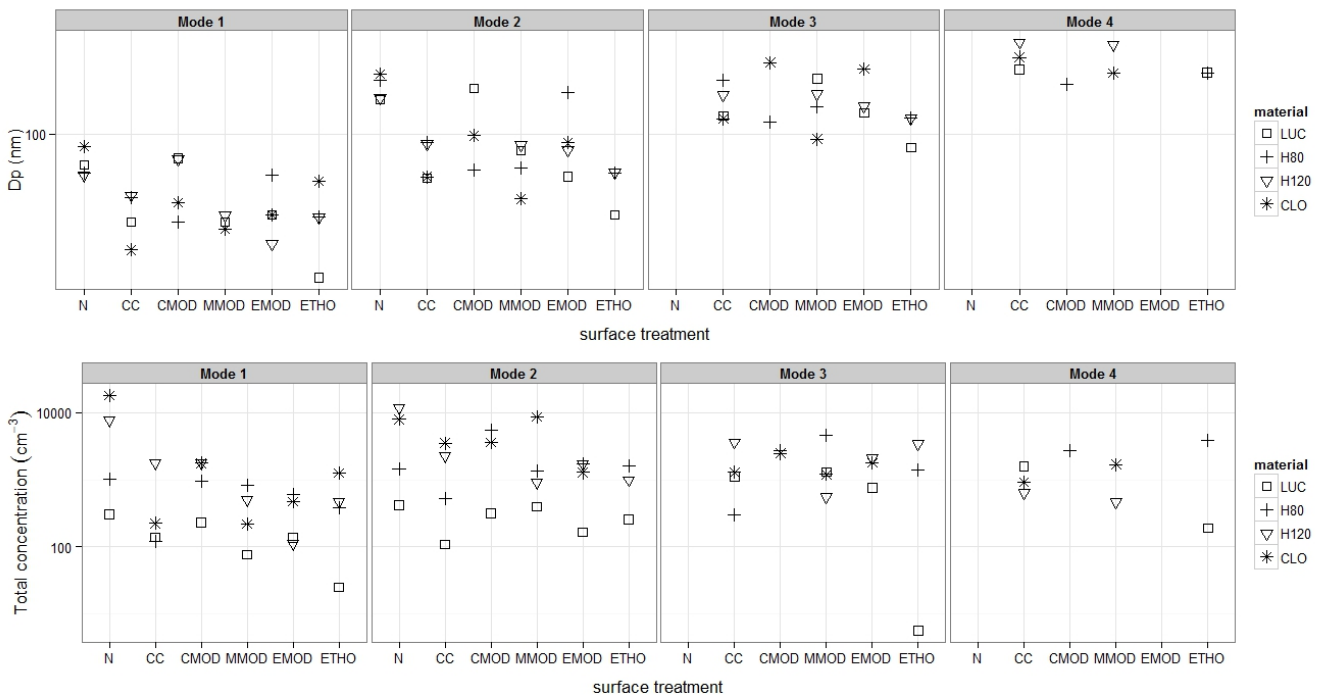

Fig. 3. Key modal characteristics of PNSDs for all materials and surface treatments obtained by multi-lognormal fitting.

in different tested materials. For instance, whilst Mode 1 of the PNSD spectra for H120-EMOD had the smallest GMD

(27 nm) compared to the other treatments applied, the GMD of the same mode for H80-EMOD was the second highest

(61 nm). This points to the importance of considering the material/surface treatment interaction as another parameter in the analysis and interpretation of the data.

Variations in the location of nanoparticle mode(s) across the surface treatments: These variations were comparable for the tested materials. The widest range of variation in nanoparticle mode(s) locations was observed in CLO samples with the range of 25–98 nm and the standard deviation of 27 nm, whilst H80 experienced the least variation, ranging from 32 nm to 90 nm (standard deviation 18 nm). H80 was the material whose nanoparticle modes were least influenced by surface treatment in terms of both location and geometric standard deviations, since neither varied significantly. To quantify the variation caused by different surface treatments in GMDs of nanoparticle modes, a categorical regression model was applied in R for each material, assuming the unmodified condition as the baseline for comparison. Table 3 presents the results of this model.

According to Table 3, deviation values are mostly negative, indicating the emission of smaller particles for the surface-treated samples compared to the unmodified ones, as was previously shown in Fig. 3. Furthermore, CC and ETHO show the most variations, as they have the highest means of absolute deviations from the baseline GMDs among the surface treatments.

Contribution of the nanoparticles to the total emissions: The ratios of the number concentration of three size ranges (nanoparticles, $100 < GMD < 300$ nm, and $GMD > 300$ nm) to the total number concentration measured for each sample are shown in Fig. 4. The concentrations of the first two ranges were measured by SMPS and the last one was measured by OPC.

Fig. 4 shows that CLO contributed the most to the emissions of nanoparticles, whilst H80 had the lowest emission of such particles amongst the tested materials. Across the surface treatments, CMOD had the most contribution to the emissions of nanoparticles, with three dominant modes in this range, i.e., more than 50% contribution to the total concentration.

As stated previously, feed rate of the milling machine was also considered as a potential driving factor influencing the particle emissions. Fig. 5 gives an overview of how the number concentrations of the emitted particles in different size ranges were affected by the feed rate of the milling machine.

According to Fig. 5, the emissions of particles did not undergo any significant variations due to the different feed rates in any of the studied size ranges, however, H80 was

shown to be affected more than LUC as the variations across the feed rates were somewhat higher in all size ranges, particularly in the first one ($d < 300$ nm). Therefore, the PNSD data obtained by the SMPS were processed and analyzed in the same way as in the previous section, in order to better understand the effect of the feed rate on the emission behavior of the submicrometer particles, with a particular interest in nanoparticles. Fig. 6 summarizes the main properties of the lognormal modes, which constitute each PNSD spectra for both tested materials and for the three tested feed rates.

It can be seen from Fig. 6 that all tested cases have two nanoparticle modes. It can also be seen that decreasing the feed rate from 1 to 3 resulted in a shift in the location of nanoparticle modes towards larger particles, however, there are some differences in how each material was affected by the feed rate. For instance, the variations in the locations of nanoparticle modes in LUC are more significant than in H80, particularly in the first mode. The same explanation used for the effect of surface treatment on the location of the nanoparticle modes could also be valid for the feed rate, associating the emission of smaller particles to the higher number of particle collisions due to the increased feed rate. In terms of the contribution of the nanoparticles to the total emissions in each case, the differences are more apparent. While the contribution of LUC nanoparticles were increased consistently by decreasing the feed rate (52%, 53%, and 60% for feed rates 1, 2, and 3, respectively), the contribution of the H80 nanoparticles reached its peak by 70% at feed rate 2, but subsequently decreased to 38% at feed rate 3.

CONCLUSIONS

This study infers the emission behavior of the synthetic clay particles from a jet milling process through analysis of the measured size distribution in a comprehensive particle size range, with a focus on the submicrometer and more particularly, nanoparticles. The suite of instruments included a SMPS for measurements of submicrometer and nanoparticles and an OPC for supermicrometer particles. The effects of the surface treatment of the clay materials and of the feed rate of the milling machine were each studied as potential driving parameters of the size distribution of the emitted particles.

The findings of this study show that the size distribution of the particles emitted from the jet milling process is significantly influenced by the surface treatment applied to the material, as well as by the feed rate of the machine. As

Table 3. Deviations from the baseline (unmodified sample) in the GMDs of nanoparticle modes due to different surface treatment.

Material	Baseline GMD (nm)	Deviation from baseline (nm)				
		CC	CMOD	MMOD	EMOD	ETHO
LUC	69	–22	6	–10.5	–20	–22
H80	63	5.5	–13	–13.5	–2	–13
H120	61	7.5	13	2	–6	–11
CLO	86	–43.5	–15	–29	–22	–29
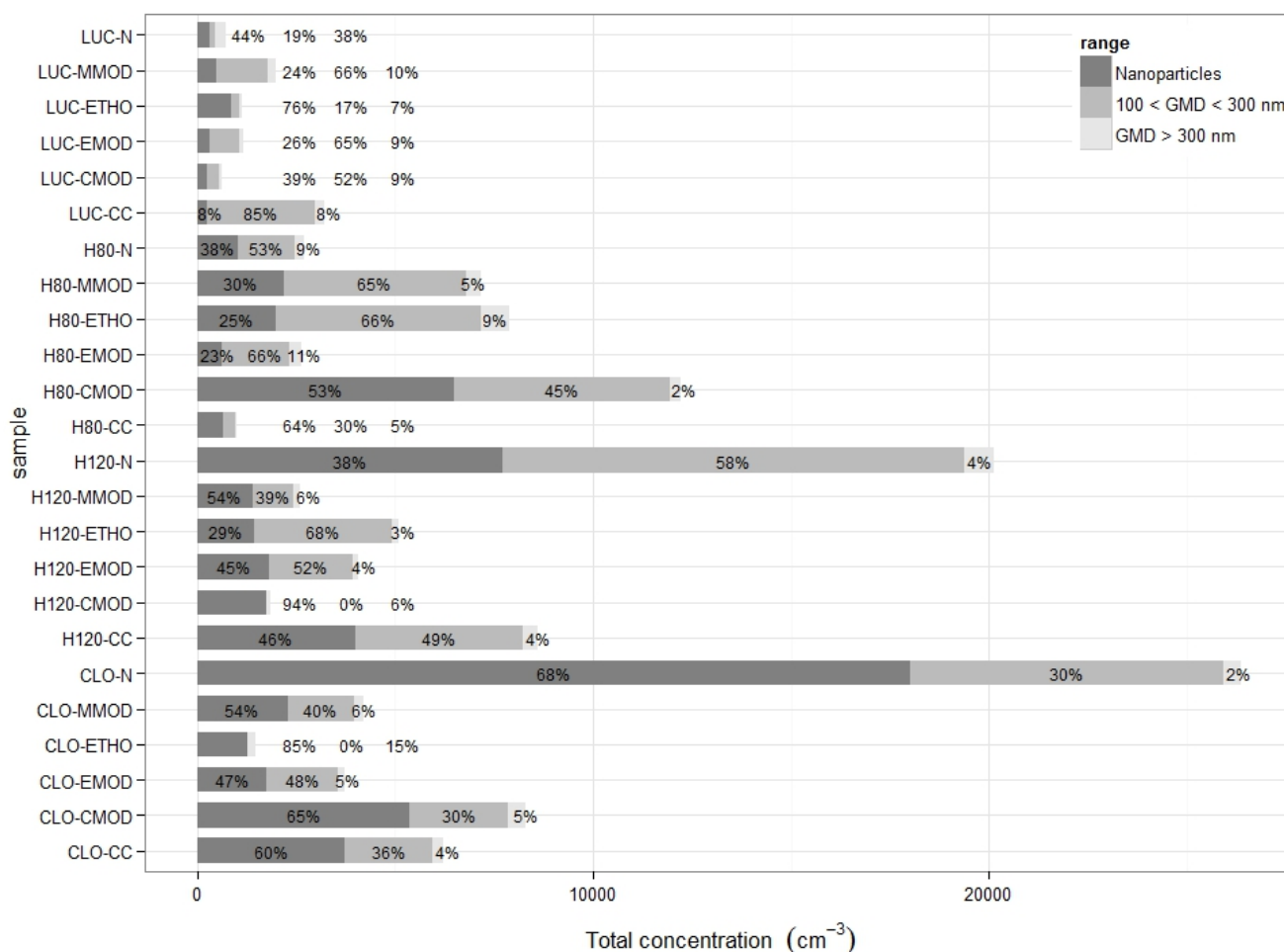
Fig. 4. Contribution of different size ranges to the total measured concentration.

the emitted particles are confirmed to be mostly nanoparticles, these effects are more significant within this size range. In terms of the emitted particle size, the general implication of the result is that applying surface treatments leads to the emission of smaller particles, as does increasing the machine feed rate. On the other hand, and regarding the contribution of nanoparticles to the emission, although the results indicated relatively high levels in many of the tested cases, no general trend was observed in the variations across either the surface treatment or the feed rate. The findings of this study signify the importance of comprehensive size distribution measurements and analysis in shedding light on the emission behavior of any types of particles from different activities, particularly nanoparticles, to provide input into the workplace exposure assessment and its regulations.

To our knowledge, the present study is the first to comprehensively analyze the emission size distribution of synthetic nanoclays, which is an important and widely-used class of materials, from a very common mechanical process. Unlike most of the similar studies, which merely focused on the effect of adding nanofillers to the reference material on the size distribution of the emitted particles, this study had a much closer look into the driving factors influencing the size distribution. The present study may be considered a step forward in size characterization of emitted nanoparticles from nanotechnology activities. A reason to support this statement is that, in contrast to some similar studies, which had difficulties in interpreting the PNSD data for nanoparticles due to different reasons such as the high levels of background particles (Koponen *et al.*, 2010; Wohlleben *et al.*, 2011;) and diffusion (Schlagenhauf *et al.*, 2012), in the present study, the emitted synthetic clay nanoparticles could be differentiated from the background efficiently and correction of the size distribution data for the background did not affect the modal properties of the PNSD spectra. Moreover, not only the findings of this study confirmed that characteristics of the materials and the operational factors have a major role in the size distribution of the emitted particles from a real-world process, the effects of these parameters were also quantified and compared across a wide range of cases.

ACKNOWLEDGMENTS
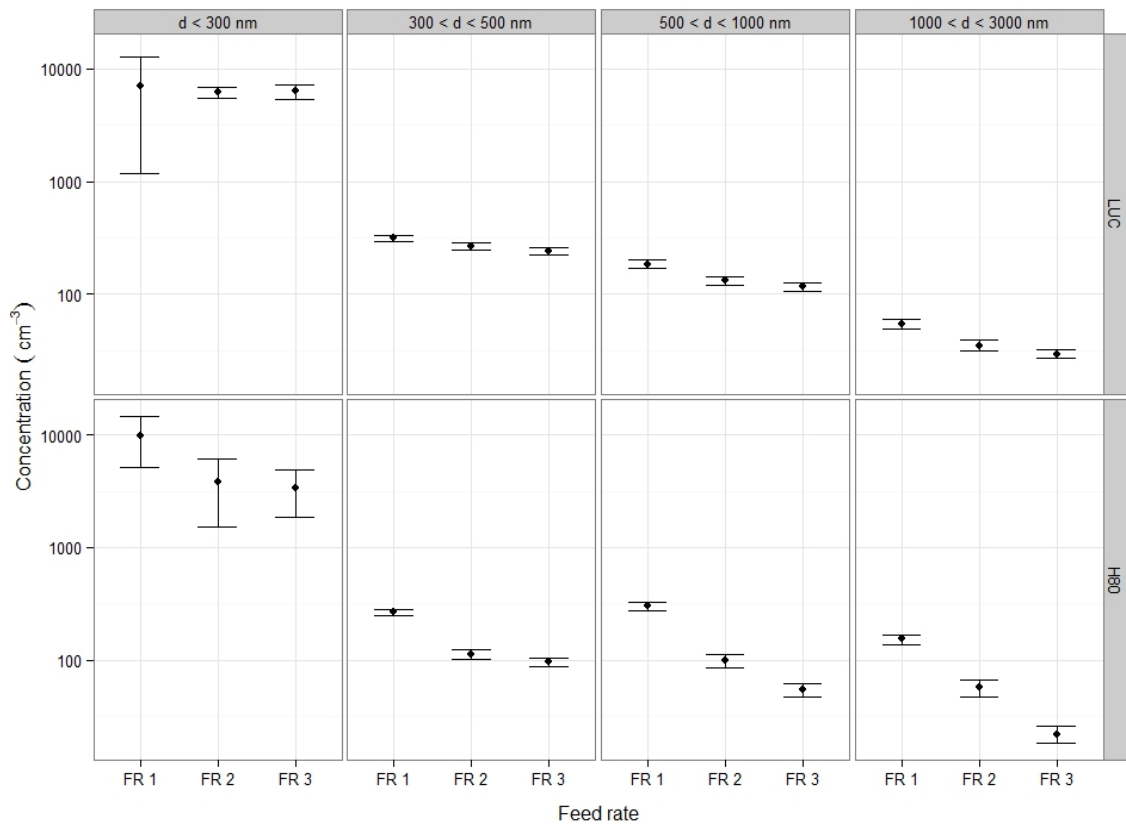
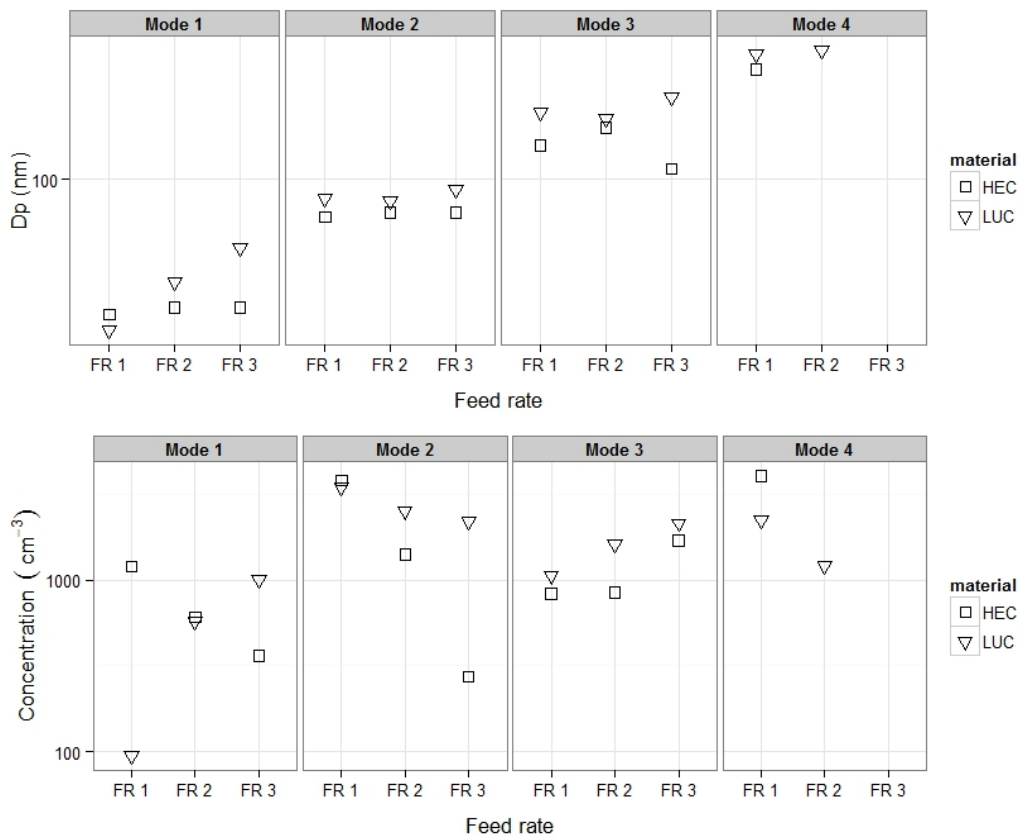**Fig. 5.** The effect of feed rate (FR 1= 7.5, FR 2 = 4.1, and FR 3 = 2.1 g min^{-1}) on number concentration of the emitted particles in different size ranges for each material.

Fig. 6. Multi-lognormal fitting results for the feed rate experiment.

REFERENCES

Asbach, C., Fissan, H., Stahlmecke, B., Kuhlbusch, T.A.J. and Pui, D.Y.H. (2008). Conceptual Limitations and Extensions of Lung-Deposited Nanoparticle Surface Area Monitor (Nsam). *J. Nanopart. Res.* 11: 101–109, doi: 10.1007/s11051-008-9479-8

Bello, D., Wardle, B.L., Yamamoto, N., Guzman deVilloria, R., Garcia, E.J., Hart, A.J., Ahn, K., Ellenbecker, M.J. and Hallock, M. (2008). Exposure to Nanoscale Particles and Fibers during Machining of Hybrid Advanced Composites Containing Carbon Nanotubes. *J. Nanopart. Res.* 11: 231–249, doi: 10.1007/s11051-008-9499-4.

Brouwer, D., Duuren-Stuurman, B., Berges, M., Jankowska, E., Bard, D. and Mark, D. (2009). From Workplace Air Measurement Results Toward Estimates of Exposure? Development of a Strategy to Assess Exposure to Manufactured Nano-objects. *J. Nanopart. Res.* 11: 1867–1881, doi: 10.1007/s11051-009-9772-1.

Brouwer, D. (2010). Exposure to Manufactured Nanoparticles in Different Workplaces. *Toxicology* 269: 120–127, doi: 10.1016/j.tox.2009.11.017

Demou, E., Peter, P. and Hellweg, S. (2008). Exposure to Manufactured Nanostructured Particles in an Industrial Pilot Plant. *Ann. Occup. Hyg.* 52: 695–706, doi: 10.1093/annhyg/men058

Donaldson, K., Aitken, R., Tran, L., Stone, V., Duffin, R., Forrest, G. and Alexander, A. (2006). Carbon Nanotubes: A Review of Their Properties in Relation to Pulmonary Toxicology and Workplace Safety. *Toxicol. Sci.* 92: 5–22, doi: 10.1093/toxsci/kfj130.

Eilers, P.H. and Marx, B.D. (1996). Flexible Smoothing with B-splines and Penalties. *Stat. Sci.* 11: 89–102.

Faghihi, E.M., Martin, D., Clifford, S., Edwards, G., He, C., Asbach, C. and Morawska, L. (2015). Are there Generalizable Trends in the Release of Airborne Synthetic Clay Nanoparticles from a Jet Milling Process? *Aerosol Air Qual. Res.* 15: 365–375.

Göhler, D., Stintz, M., Hillemann, L. and Vorbau, M. (2010). Characterization of Nanoparticle Release from Surface Coatings by the Simulation of a Sanding Process. *Ann. Occup. Hyg.* 54: 615–624, doi: 10.1093/annhyg/meq053.

Hinds, W.C. (2012). *Aerosol Technology: Properties, Behavior, and Measurement of Airborne Particles*. John Wiley & Sons,

Hussein, T., Dal Maso, M., Petäjä, T., Koponen, I.K., Paatero, P., Aalto, P.P., Hämeri, K. and Kulmala, M. (2005). Evaluation of an Automatic Algorithm for Fitting the Particle Number Size Distributions. *Boreal Environ. Res.* 10: 337–355.

Koponen, I., Jensen, K. and Schneider, T. (2009). Sanding Dust from Nanoparticle-containing Paints: Physical Characterisation. *J. Phys. Conf. Ser.* 151: 012048.

Koponen, I.K., Jensen, K.A. and Schneider, T. (2010). Comparison of Dust Released from Sanding Conventional and Nanoparticle-doped Wall and Wood Coatings. *J. Exposure Sci. Environ. Epidemiol.* 21: 408–418.

Kuhlbusch, T., Asbach, C., Fissan, H., Gohler, D. and Stintz, M. (2011). Nanoparticle Exposure at Nanotechnology Workplaces: A Review. *Part. Fibre Toxicol.* 8: 22.

Maynard, A. and Kuempel, E. (2005). Airborne Nanostructured Particles and Occupational Health. *J. Nanopart. Res.* 7: 587–614, doi: 10.1007/s11051-005-6770-9

Maynard, A.D. and Aitken, R.J. (2007). Assessing Exposure to Airborne Nanomaterials: Current Abilities and Future Requirements. *Nanotoxicology* 1: 26–41, doi: 10.1080/17435390701314720

Methner, M., Hodson, L., Dames, A. and Geraci, C. (2010). Nanoparticle Emission Assessment Technique (NEAT) for the Identification and Measurement of Potential Inhalation Exposure to Engineered Nanomaterials - Part B: Results of 12 Field Studies. *J. Occup. Environ. Hyg.* 7: 163–176.

Ono-Ogasawara, M., Serita, F. and Takaya, M. (2009). Distinguishing Nanomaterial Particles from Background Airborne Particulate Matter for Quantitative Exposure Assessment. *J. Nanopart. Res.* 11: 1651–1659, doi: 10.1007/s11051-009-9703-1.

Park, J., Ramachandran, G., Raynor, P. and Kim, S. (2011). Estimation of Surface Area Concentration of Workplace Incidental Nanoparticles Based on Number and Mass Concentrations. *J. Nanopart. Res.* 13: 4897–4911

R.Core.Team (2013). R: A Language and Environment for Statistical Computing. R Foundation for Statistical Computing.

Ramachandran, G. and Cooper, D.W. (2011). Size Distribution Data Analysis and Presentation. In *Aerosol Measurement*. John Wiley & Sons, Inc., pp. 479–506. doi: 10.1002/9781118001684.ch22.

Sachse, S., Silva, F., Zhu, H., Irfan, A., Leszczynska, A., Pielichowski, K., Ermini, V., Blazquez, M., Kuzmenko, O. and Njuguna, J. (2012). The Effect of Nanoclay on Dust Generation during Drilling of PA6 Nanocomposites. *J. Nanomaterials* 2012: 26–26, doi: 10.1155/2012/189386.

Schlagenhauf, L., Chu, B.T.T., Buha, J., Nüesch, F. and Wang, J. (2012). Release of Carbon Nanotubes from an Epoxy-Based Nanocomposite during an Abrasion Process. *Environ. Sci. Technol.* 46: 7366–7372, doi: 10.1021/es 300320y

Stoeffler, K., Lafleur, P.G. and Denault, J. (2008). Thermal Decomposition of Various Alkyl Onium Organoclays: Effect on Polyethylene Terephthalate Nanocomposites' Properties. *Polym. Degrad. Stab.* 93: 1332–1350, doi: 10.1016/j.polymdegradstab.2008.03.029

Suh, W.H., Suslick, K.S., Stucky, G.D. and Suh, Y.H. (2009). Nanotechnology, Nanotoxicology, and Neuroscience. *Prog. Neurobiol.* 87: 133–170, doi: 10.1016/j.pneurobio.2008.09.009

Tsai, C.J., Huang, C.Y., Chen, S.C., Ho, C.E., Huang, C.H., Chen, S.W., Chang, C.P., Tsai, S.J. and Ellenbecker, M.J. (2011). Exposure Assessment of Nano-sized and Respirable Particles at Different Workplaces. *J. Nanopart. Res.* 13: 4161–4172.

Tsai, S.J., Ashter, A., Ada, E., Mead, J.L., Barry, C.F. and Ellenbecker, M.J. (2008). Control of Airborne Nanoparticles Release during Compounding of Polymer Nanocomposites. *Nano* 03: 301–309, doi: 10.1142/S179

329200800112X

Tsai, S.J., Hofmann, M., Hallock, M., Ada, E., Kong, J. and Ellenbecker, M. (2009). Characterization and Evaluation of Nanoparticle Release during the Synthesis of Single-Walled and Multiwalled Carbon Nanotubes by Chemical Vapor Deposition. *Environ. Sci. Technol.* 43: 6017–6023, doi:10.1021/es900486y

WaveMetrics. Lake Oswego, OR, USA.

Wohlleben, W., Brill, S., Meier, M.W., Mertler, M., Cox, G., Hirth, S., Vacano, B.V., Strauss, V., Treumann, S., Wiench, K., Ma-Hock, L. and Landsiedel, R. (2011). On the Lifecycle of Nanocomposites: Comparing Released Fragments and their In-Vivo Hazards from Three Release Mechanisms and Four Nanocomposites. *Small* 7: 2384–2395, doi: 10.1002/smll.201002054,

Wood, S.N. (2003). Thin Plate Regression Splines. *J. R. Stat. Soc. Series B* 65: 95–114.